International Journal of Heat and Fluid Flow 31 (2010) 32–44

Contents lists available at ScienceDirect

International Journal of Heat and Fluid Flow

journal homepage: www.elsevier.com/locate/ijhff

Experimental study and large eddy simulation of turbulent flow around tube bundles composed of wavy and circular cylinders

K. Lam [a,*], Y.F. Lin [a], L. Zou [b], Y. Liu [a]

[a] Department of Mechanical Engineering, The Hong Kong Polytechnic University, Hung Hom, Kowloon, Hong Kong
[b] School of Mechanical and Electronic Engineering, Wuhan University of Technology, Wuhan 430070, PR China

ARTICLE INFO

Article history:
Received 4 November 2008
Received in revised form 19 October 2009
Accepted 21 October 2009
Available online 18 November 2009

Keywords:
Tube bundles
Wavy cylinders
Turbulent flow
Large eddy simulation
LDA

ABSTRACT

This paper presents the results of an investigation on the effects of wavy cylindrical tubes in a staggered heat exchanger tube bundle. Experimental measurements and large eddy simulation (LES) technique were used to study the turbulent flow characteristics in a staggered tube bundle arrangement at a sub-critical Reynolds number of Re = 7500. The aim of this investigation is to compare the flow characteristics of a new configuration of cylindrical tubes with that of a similar arrangement which comprises purely circular cylinders. The first row of circular tubes is replaced by a row of wavy cylindrical tubes. The result of the experiment shows that the mean velocity distributions and turbulence intensity, obtained by the present LES method, are in good agreement with the Laser Doppler Anemometer (LDA) measurements. The wake patterns around the second row of cylinders become more well organized upon the introduction of wavy cylinders of optimal wavelength ($\lambda/D_m = 6$). The turbulent kinetic energy behind the first row of tubes is also reduced. The power density spectra of the vortex shedding in the tube bundle are evidently suppressed. As a result, the fluctuating forces of the tube bundles are weakened. However, the drag is not noticeably reduced by such modification.

1. Introduction

Tube bundles are widely employed in cross-flow heat exchangers. The complex vortex shedding characteristics behind the cylindrical tubing can cause severe vibration of the tubes, generally known as flow-induced vibration (FIV). FIV of heat exchanger tube bundles may cause serious structural failure. Over the past years, numerous experimental investigations have been carried out to study the mechanism of FIV in different configurations of tube bundles. Austermann and Popp (1995) investigated the fluid elastic instability in different tube arrays. They found that stability depends on the pattern of tube arrays and on the space ratio of tube. Price et al. (1995) reported the vortex shedding characteristics of tube arrays that were obtained by flow visualization methods. Romberg and Popp (1998a,b) conducted experimental investigations on the stability factors of normal and rotated triangular tube arrays with different pitch-to-diameter ratios. Chen and Srikantiah (2001) presented series of experiments to measure motion-dependent fluid forces for various tube arrays. Rottmann and Popp (2003) further investigated the influence of approach flow on the first row of tube bundles. Paul et al. (2007) preformed measurements in a staggered tube bundle with fixed pitch-to-diameter ratios at sub-critical Reynolds number using the particle image velocimetry technique. Their results showed that the flow exhibits strong Reynolds number dependence in the developing region, however no significant Reynolds number effect could be observed in the spatially periodic region.

Because of the complicated flow characteristics in the heat exchanger tube bundles, the vortex structures cannot be clearly observed and a lot of valuable information cannot be obtained by experimental techniques alone. It is then suggested that numerical simulations should be able to capture the instantaneous three-dimensional vortex structures and other instantaneous fluid dynamic parameters, such as drag, lift, pressure, velocity and Reynolds stress. Successful numerical investigations of flow around tube bundles had been carried out by Bouris and Bergeles (1999), Watterson et al. (1999), Beale and Spalding (1999), Sweeney and Meskell (2003), Schneider and Farge (2005), Lam et al. (2006) and Paul et al. (2008) using different numerical methods. For turbulent flow, large eddy simulation (LES) has become a very popular and reliable numerical method, with which the complex turbulent flow characteristics can be captured accurately. For example, Barsamian and Hassan (1997) examined the non-staggered and staggered tube bundles using the two-dimensional LES method. Rollet-Miet et al. (1999) developed a finite element LES code compared with the Reynolds Averaged Navier–Stokes (RANS) equation. Recently, Liang and Papadakis (2007) also confirmed that the

* Corresponding author. Tel.: +852 2766 6649; fax: +852 2365 4703.
E-mail address: mmklam@polyu.edu.hk (K. Lam).

0142-727X/$ - see front matter © 2009 Elsevier Inc. All rights reserved.
doi:10.1016/j.ijheatfluidflow.2009.10.006

Nomenclature

a	wave amplitude of a wavy cylinder (m)
C_s	Smagorinsky constant, dimensionless
D_m	mean diameter of a wavy cylinder (m)
D_{max}	maximum diameter of a wavy cylinder (m)
D_{min}	minimum diameter of a wavy cylinder (m)
D_z	local diameter of a wavy cylinder (m)
FFT	Fast Fourier Transform
F_D, F_L	total drag force, total lift force (N)
f_s	vortex shedding frequency (Hz)
LDA	Laser Doppler Anemometer
LES	large eddy simulation
L_x, L_y, L_z	computational domain (m)
$\bar{p}$	pressure (Pa)
Re	Reynolds number, dimensionless
SGS	subgrid-scale
St	Strouhal number, dimensionless
t	time (s)
Δt	time step, dimensionless
TKE	turbulent kinetic energy (m^2/s^2)
$\bar{u}_i$	filtered velocity component (m/s)
U, V, W	velocity components (m/s)
u', v', w'	root-mean-square velocity (m/s)
U_c	convection velocity (m/s)
U_∞	incoming flow velocity (m/s)
x, y, z	cartesian coordinate system
y^+	non-dimensional cell distance from wall

Greek symbols

λ	spanwise wavelength of a wavy cylinder (m)
λ_z	spanwise wavelength of the streamwise vortices (m)
ν	kinematic viscosity (m^2/s)
ρ	fluid density (kg/m^3)
τ_{ij}	subgrid-scale stress (m^2/s^2)

results by LES method are in very good agreement with the LDA measurements on the investigation of turbulent flow around staggered tube bundles. Important information such as instantaneous velocity field, force characteristics, etc. were obtained. All of the above showed that both the experimental measurement and numerical simulation are useful complementary tools for the study of FIV.

Although some interesting studies which are based on the premise of modified tube shapes have been carried out, most of the investigations have focused on the characteristics of fluidelastic instability of tube bundles with the circular cylinders. In our previous investigation, it was found that a cylinder with wavy surface can weaken, to the extent that it may even suppress the FIV comparing with a circular cylinder at the same Reynolds numbers (Lam et al., 2004a,b). An optimal spanwise wavelength ratio $\lambda/D_m \approx 6$ for drag reduction and fluctuating lift suppression was found at low Reynolds number of 100 over a wide wavelength range by Lam and Lin (2007, 2009). For turbulent flow, Lam and Lin (2008) found an optimal wavelength $\lambda/D_m \approx 2$ using the large eddy simulations over a narrow wavelength range. Significant drag force reduction and weakening of vibration were found at Re = 3000. An extension of investigation on flow past a row of wavy cylinders conducted by Lam et al. (2007) showed that the wavy cylinders give rise to a more stable flow pattern with less fluctuation and longer wake vortex closure length compared with a row of circular cylinder.

Based on the results of the aforementioned experiments, the present investigation aims at controlling FIV of the tube bundles using different combinations of wavy and circular cylinders. It is hoped that by replacing certain circular cylinders with wavy cylinders in tube bundle, flow-induced vibration could be minimized or suppressed. The finite-volume method (FVM) is employed to simulate the flow past the wavy and circular tube bundles. For the study of turbulent flow, the large eddy simulation (LES) is adopted. Also, experimental measurements using the Laser Doppler Anemometer (LDA) technique were performed to supplement the study. The time-average velocity distributions of the flow field are obtained. The forces on the cylinders were measured using a three-component quartz piezoelectric load cell so that the numerical results can be confirmed.

2. Experimental setup and measurement procedure

The present experiments were carried out in a closed-loop water tunnel with a test section of 2.1 m × 0.15 m × 0.3 m (length, width, height) with correspondence to the direction of x, y and z, respectively. Two pumps with one electric control system were used to produce a desired main flow velocity in the test section, while the free stream velocity in the testing area could be continuously adjusted from 0 to 4 m/s. Numbers are assigned to the staggered set of tubes. Numbers 1–5 denote the first row in the upstream position while, numbers 6–9 and 10–14 denote second row and the third rowing tubing, respectively. The tubes height for the present experiment is $15D_m$. Fig. 1 shows the schematic experimental setup of the tube bundle. The flow characteristic is studied with the first row of tubes replaced by five wavy cylinders (a cylinder with a varying circular cross section along the spanwise direction) as opposed to a configuration of purely circular cylinders (a cylinder with a constant circular cross section along the spanwise direction). Lam et al. (2007) experimentally investigated turbulent flow around a row of side by side wavy cylinders with a fixed spacing ratio of $1.5D_m$. Both the in-phase and out-of-phase arrangement of the wavy cylinders were studied. The results show that the out-of-phase arrangement of the wavy cylinders gives rise to a more stable flow pattern with less fluctuation. As shown in Fig. 1b, the first row of wavy cylinders is arranged to be out-of-phase according to our previous study. Following the same study, the spacing ratio between the tubes rows is fixed at $1.5D_m$ (crosswise direction, y-direction). As the vortex shedding of the wavy cylinder occurs at further downstream compared with a circular cylinder (Lam and Lin, 2008, 2009), we extend the streamwise (x-direction) spacing ratio of the tubes in each tube rows to a fixed value of $2.5D_m$ (see Fig. 2a). The geometry of the wavy cylinders can be described by the following equation,

$$D_z = D_m + 2a\cos(2\pi z/\lambda) \tag{1}$$

Here, D_z denotes the local diameter of the wavy cylinder and the mean diameter can be calculated with the equation $D_m = (D_{min} + D_{max})/2$. D_{min} represents the minimum diameter of cylinder along the spanwise direction, while D_{max} represents the maximum diameter of the wavy cylinder. The amplitude of the curve surface is denoted by 'a', and 'λ' is the wavelength along the spanwise direction. The axial locations with maximum local diameter are termed 'nodes', while the axial locations of the minimum diameter are called 'saddles'. In the present investigation, two wavelength ratios with $\lambda/D_m = 1.5$ and $\lambda/D_m = 6$ were employed with a fixed wave amplitude of $a/D_m = 0.15$ (see Table 1). A tube bundle (Model-I) with pure circular cylinder in the first row is first investigated for comparison.

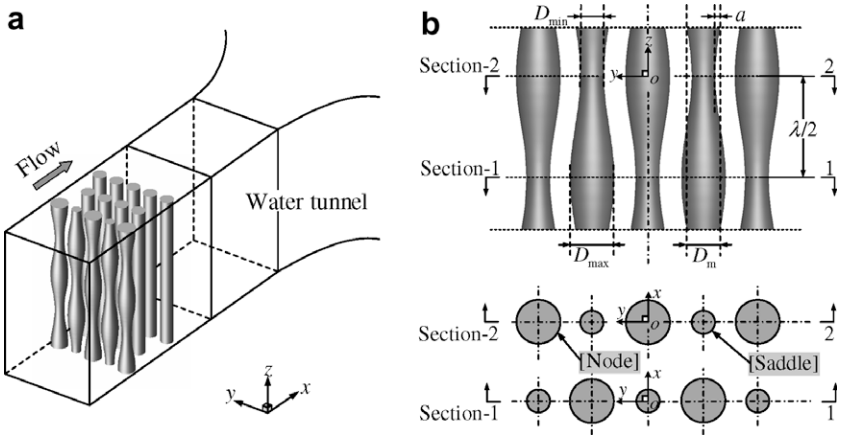

Fig. 1. (a) Experimental setup of the tube bundle. (b) Schematic of the out-of-phase arrangement of wavy cylinders in the first row of the tube bundle.

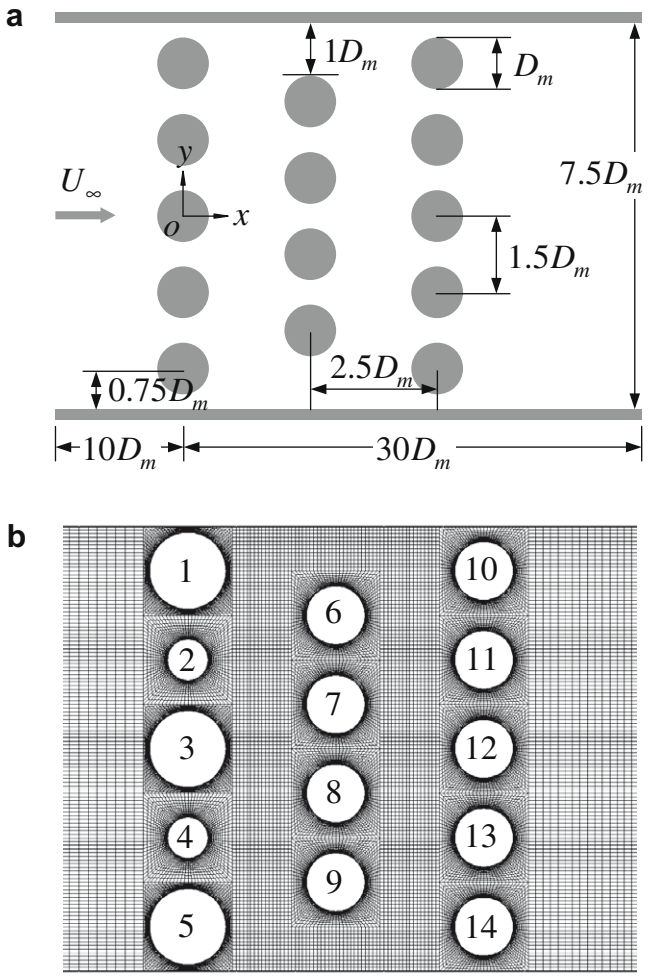

Fig. 2. Sketch of tube bundle arrangement: (a) tube bundles arrangement and (b) computational gird of the tube bundle with wavy cylinders in the first row.

The position of the first row cylinders is 0.2 m from the upper wall of the water tunnel test section. The cylinders of the mean diameter D_m = 0.02 m with the height of 0.297 m (resulting in aspect ratios of 14.85) were set in the test section. The incoming flow velocity U_∞ is 0.38 m/s, corresponding to the Reynolds number of 7500 (based on the mean diameter of wavy cylinder, $Re = D_m U_\infty / \nu$). At this U_∞, the free-stream turbulent intensity was about 2%. All geometrical lengths are scaled by D_m.

Table 1
Tube bundles models: CY = circular cylinder; WY = wavy cylinder.

Tube bundles	Row-1		Row-2	Row-3
Model-I	CY (1–5)	$\lambda/D_m = \infty$ $a/D_m = 0$	CY (6–9)	CY (10–14)
Model-II	WY (1–5)	$\lambda/D_m = 6.0$ $a/D_m = 0.15$	CY (6–9)	CY (10–14)
Model-III	WY (1–5)	$\lambda/D_m = 1.5$ $a/D_m = 0.15$	CY (6–9)	CY (10–14)

In order to obtain the quantitative mean and fluctuating velocity distributions for turbulent flow around the tube bundles, a two-colour fibre-optic LDA (Dantec Model 58N40 LDA with enhanced FVA signal processor) was employed in the present investigations. The LDA system is equipped with software for data processing and analysis. The LDA measuring volume has a minor axis 1.18 mm and a major axis of 2.48 mm. The uncertainties in mean velocity (both of the streamwise and transverse velocities components) and turbulence intensity are estimated to be ±3% and ±7%, respectively, for detail uncertainty analysis, refer Wang et al. (2005). The higher errors generally occur in the regions with steep velocity gradients. For each data-point, 50,000 validated samples were acquired with a data rate of 0.8–4 kHz. For similar LDA measurements on tube bundles by Balabani and Yianneskis (1996), as reported by Liang and Papadakis (2007), the uncertainty in mean velocity and turbulence quantities are, respectively, 1–5% and 5–10%.

Furthermore, forces on the cylinders were measured using a three-component quartz piezoelectric load cell characterized by high response, resolution and stiffness. The load cell mounted on the top end of the wavy cylinder is bolted tightly between two stainless machine-polished steel blocks. Static calibrations of the load cell in the lift and drag directions were carried out using dead weights. It could be seen that the load cell had a high linearity in the load/output relation. Moreover, for the force measurements, the test cylinder was cantilever-mounted. The distance between the cylinder lower end and the bottom wall is about 0.003 m. For the present study the uncertainty in drag is about ±5%, while that of fluctuating lift is approximately ±12%.

3. Computational models

3.1. Governing equations

By using the three-dimensional LES turbulence model, the large-scale eddies are solved directly by the filtered Navier–Stokes

equations, and the small eddies are modeled using a subgrid-scale (SGS) model. The large-scale turbulence motions are strongly dependent on the flow geometry and boundary conditions, and they can be predicted by the resolved flow in the LES method. On the other hand, the subgrid-scale model represents the small-scale eddy motion which is more universal in character than the large-scale eddy.

By applying the filtering operation, the incompressible Navier–Stokes equations for the evolution of the large-scale motions can be obtained. The governing equations employed for LES are

$$\frac{\partial \bar{u}_i}{\partial x_i} = 0, \tag{2}$$

$$\frac{\partial \bar{u}_i}{\partial t} + \frac{\partial \bar{u}_i \bar{u}_j}{\partial x_j} = -\frac{1}{\rho}\frac{\partial \bar{p}}{\partial x_i} + \nu \frac{\partial^2 \bar{u}_i}{\partial x_j \partial x_j} - \frac{\partial \tau_{ij}}{\partial x_j}, \quad (i = 1,2,3) \tag{3}$$

where $\bar{u}_i$ is the filtered velocity component along the Cartesian coordinates x_i, $\bar{p}$ the pressure, ρ the fluid density and ν is the kinematic viscosity of the fluid. The influence of the small scales on the large (resolved) scales is exerted through the subgrid-scale stress which could be defined by

$$\tau_{ij} = \overline{u_i u_j} - \bar{u}_i \bar{u}_j, \tag{4}$$

which are unknowns and must be modeled with a subgrid model. The Smagorinsky constant, $C_s = 0.12$, was adopted by Barsamian and Hassan (1997) in turbulent flow around tube bundle. Moreover, Liang and Papadakis (2007) used $C_s = 0.1$ to investigate turbulent flow around a staggered tube bundle at Re = 8600. As a result, all computations in the present work were carried out with a Smagorinsky constant, $C_s = 0.1$, which is found to be a suitable value for the applications of the Smagorinsky model to turbulent wake simulation.

Detailed descriptions of the present LES method can be found in Lam and Lin (2008). The finite-volume method (FVM) applied on unstructured grids has been employed to solve the unsteady incompressible Navier–Stokes equations. A second-order central differencing scheme is used for momentum discretization while a second-order implicit scheme is employed to advance the equations in time. The pressure implicit method with splitting of operators (PISO) algorithm is used to deal with the pressure–velocity coupling between the momentum and the continuity equations.

3.2. Computational domain and boundary conditions

The computational domain is set at $L_x \times L_y \times L_z$ in the x-, y-, z-directions of a fixed Cartesian coordinate system. A tube bundle model is built inside it. The origin of the coordinate system is located at the central position of the wavy tubes (see Fig. 1b). The x-axis is aligned with the inlet flow direction (streamwise direction), the z-axis is parallel to the cylinder axis (spanwise direction) and the y-axis lies perpendicular to both the x- and z-axes (crosswise direction).

In the present simulations, the computational boundaries L_x and L_y are set at $40D_m$ and $7.5D_m$, respectively (refer to the experimental setup). The upstream boundary is set at $10D_m$ (determined from the experiment) before the centerline of the first row of tubes. The downstream boundary is $25D_m$ away from the third row of tubes. The experimental studies of Williamson et al. (1995) and Williamson (1996) showed that the wavelength scales of the streamwise vortex structures in the near wake of a circular cylinder is given by $\lambda_z/D_m \approx 25\mathrm{Re}^{-1/2}$. Here, λ_z is the spanwise wavelength of the vortices and the estimated near wake wavelength of streamwise vortices for the circular cylinder is around $0.3D_m$ for a fixed Reynolds number of 7500. Further downstream, the large-scale structures for streamwise vortices with wavelengths $\lambda_z/D_m \approx 1$ have been reported (Williamson, 1996). Considering the resolution of the large-scale eddies, we use $L_z = 3D_m$ for the Model-I tube bundles in the spanwise direction is considered to be sufficient for the present simulations of the circular cylinder (see Table 2). As mentioned by Lam et al. (2004b) and Zhang et al. (2005), for single wavy cylinder, the periodic vortex structures were experimentally observed to be consistent with the periodic repetition of wavy cylinder of spanwise wavelength, λ. Recently, Lam and Lin (2007, 2008, 2009) captured this kind of phenomenon using the numerical method for both laminar flow and turbulent flow. Lam et al. (2007) discovered this kind of periodic repetition of vortex structure along the spanwise direction of a row of out-of-phase arrangement wavy cylinders. In the present simulation, the spanwise domain L_z of the Model-II tube bundles is $6D_m$, or is equal to one wavelength λ of the wavy cylinder ($\lambda/D_m = 6$). While, L_z of the Model-III tube bundles is $3D_m$, or equal to two wavelengths 2λ ($\lambda/D_m = 1.5$).

Table 2
Details of grid model for different tube bundles (*Nc*: cylinder circumference mesh numbers; *Nz*: spanwise mesh layers).

Model	Case	Grid	*Nc*	*Nz*	$L_x \times L_y \times L_z$ (D_m)
Model-I	Grid-I	10,20,096	80	28	$40 \times 7.5 \times 3$
	Grid-II	14,26,944	96	32	$40 \times 7.5 \times 3$
Model-II	Grid-I	20,40,192	80	56	$40 \times 7.5 \times 6$
	Grid-II	28,53,888	96	64	$40 \times 7.5 \times 6$
Model-III	Grid-II	14,26,944	96	32	$40 \times 7.5 \times 3$

The computational domain is divided into a number of unstructured hexahedral grids. The grid is non-uniform in the x–y plane (see Fig. 2b), but uniform along the z-direction. The grids are clustered near the cylinder surface and the spacing is properly increased in a ratio of 1.1 away from the cylinder. The distance from the cylinder surface to the nearest grid points is fixed at y^+ close to 1. At the inlet boundary, a uniform velocity profile ($u = 1$, $v = w = 0$) is imposed. Moreover, base on the experimental data, at the inlet the relative turbulence intensity is set equal to 2%. A convective boundary condition ($\partial u_i/\partial t + U_c(\partial u_i/\partial x) = 0$) is used at the outlet boundary (Breuer (1998), Sohankar et al. (2000), Lam and Lin (2008)), where U_c is the convection velocity equal to the mean velocity at the inlet. The no-slip boundary condition ($u = v = w = 0$) is prescribed at the surface of the cylinders and the lateral sides of the domain. The periodic boundary condition is employed at the boundaries in the spanwise direction to reduce the computational time. A validation test is also performed prior to the present simulations.

A non-dimensional time step $\Delta t U_\infty/D_m = 0.02$ was chosen for the simulation, yielding the maximum CFL number close to two and ensuring sufficiently small CFL numbers of less than 1 for most part of the computational domain. It was dictated by the numerical stability of the computations. For all of the present simulations, at least 150 dimensionless time units (tU_∞/D_m), in correspondence with around 30 vortex-shedding cycles, were taken in order to obtain more reliable statistical average information.

4. Results and discussion

4.1. Single wavy cylinder test

On the study of turbulent flow characteristics, the previous investigation by Lam et al. (2004a) focused mainly on the effects of wavy cylinders with relatively short wavelengths ($\lambda/D_m \leqslant 3.3$). Lam et al. (2004a) measured the mean and fluctuating forces of wavy cylinders with $\lambda/D_m = 1.5$–2.3 at sub-critical Reynolds numbers from 20,000 to 50,000. Results indicated a maximum drag reduction up to 20%. By using the LES method, Lam and Lin

(2008) found that a wavy cylinder with λ/D_m of around 1.9 can lead to significant drag force reduction and vibration suppression at Re = 3000. For laminar flow, however, Lam and Lin (2007, 2009) numerically investigated the flow around wavy cylinders at Re = 100 over a wide range of spanwise wavelength. Two optimal wavelengths for drag reduction were found at $\lambda/D_m \approx 2$ and $\lambda/D_m \approx 6$. With a larger value of spanwise wavelength $\lambda/D_m = 6$, the vortex shedding behind the wavy cylinder was greatly suppressed and the drag force was evidently reduced. This observation is consistent with the findings of Darekar and Sherwin (2001). They investigated a wavy square cylinder at low Reynolds numbers. The optimal wavelength obtained was around $5.7D_m$. Similarly, Bearman and Owen (1998) also measured the wavy square cylinder at high Reynolds number. Their report showed that there was also evidence of drag reduction. Henceforth, it was determined that $\lambda/D_m = 6$ was the correct optimal wavelength for the suppression of FIV.

Considering the results above, it is anticipated that the introduction of wavy cylinders with $\lambda/D_m = 6$ would give better effects in FIV suppression. To confirm that $\lambda/D_m = 6$ is the optimal wavelength required at sub-critical Reynolds numbers, we first performed force measurements of a wavy cylinder with wavelength ratio ($\lambda/D_m = 6$) at Re from 6800 to 13,400. At the same time, the large eddy simulation of flow around a single wavy cylinder ($\lambda/D_m = 6$, $a/D_m = 0.15$) at Re = 7500 was also performed for comparison.

Fig. 3 shows the force coefficients of wavy cylinder ($\lambda/D_m = 6$, $a/D_m = 0.15$) obtained by the present load cell measurements and large eddy simulation compared with that of a circular cylinder within the same range of Reynolds numbers. The overall drag coefficient is defined with the equation, $C_D = 2F_D/\rho U_\infty^2 D_m L_z$, while the value of the overall lift coefficient can be determined by $C_L = 2F_L/\rho U_\infty^2 D_m L_z$. The total drag and total lift are designated as F_D and F_L, respectively. The mean drag coefficients of a circular cylinder ($\bar{C}_D$) obtained by load cell measurements are in good agreement with the experimental results by Zdravkovich (1997). All the values of $\bar{C}_D$ for circular cylinders measured at the Reynolds numbers from 6800 to 13,400 are approximately 1.1 (see Fig. 3a). The values of $\bar{C}_D$ for the wavy cylinder ($\lambda/D_m = 6$, $a/D_m = 0.15$), however, are evidently smaller than those of a circular cylinder within the same Reynolds number range. A result of drag reduction up to 18% could be observed. The values of $\bar{C}_D$ obtained from the LES method for both wavy and circular cylinders are slightly large than those of the measured results. However, the drag reduction of the wavy cylinder of about 17.3% is obtained. This value is close to the experimental result (see Fig. 3a). The fluctuating lift coefficients captured by load cell technique (C_L', root-mean-square value) are also in good agreement with the empirical results obtained by Norberg (2003). The values of C_L' for the wavy cylinders are also smaller than that of a circular cylinder at the same Reynolds number. About 75% reduction of fluctuating lift coefficients is obtained. By the LES method, however, the values of C_L' for both wavy and circular cylinders are smaller than that of the experimental results. The reduction of C_L' for the wavy cylinder is up to 85%, which is slightly lower than the load cell measurements (see Fig. 3b). The difference may due to the effect on the periodic boundary condition used by LES method (two wavelengths for the wavy cylinder, resulting in the aspect ratio of 12) and the finite length of the cylinder models by load cell measurements (an aspect ratio of 14.85 for the experimental set up). In general, it is concluded that the present LES

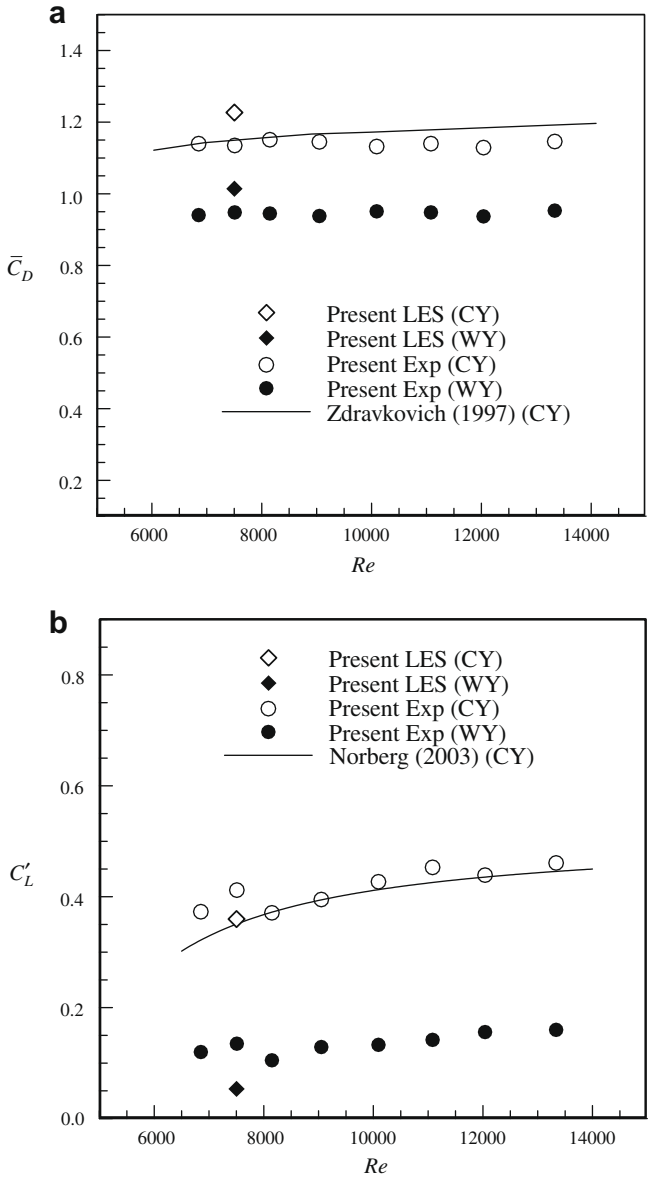

Fig. 3. Force coefficients for a wavy cylinder ($\lambda/D_m = 6$, $a/D_m = 0.15$) compared with a circular cylinder at sub-critical Reynolds numbers. (a) Mean drag coefficients and (b) fluctuating lift coefficients.

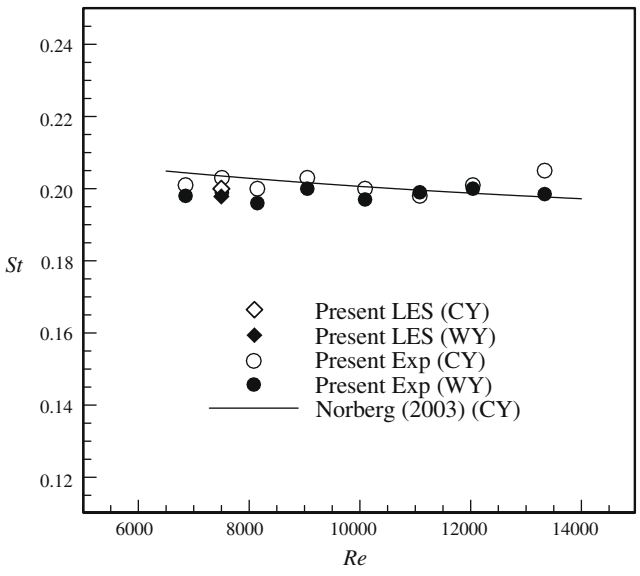

Fig. 4. Strouhal numbers for a wavy cylinder ($\lambda/D_m = 6$, $a/D_m = 0.15$) compared with a circular cylinder at sub-critical Reynolds numbers.

method can well predict the characteristic of flow past a wavy cylinder. Both the experimental and numerical results confirmed that the wavy cylinder of $\lambda/D_m = 6$ is a suitable choice for the control of flow-induced vibration.

Fig. 4 shows the Strouhal numbers ($St = f_s D_m/U_\infty$) of a circular cylinder and wavy cylinder obtained from the load cell measurements and LES calculations. The characteristics of the circular cylinder also agree with the results of the empirical relation summarized by Norberg (2003). Here, f_s is the vortex shedding frequency. Within this sub-critical Reynolds number range, both the Strouhal numbers of the wavy cylinders and circular cylinder are approximately equal to 0.21. The results are the same as that obtained by Lam et al. (2004a) and Lam and Lin (2008). They found that the wavy shapes have little effect on the frequency characteristics of vortex shedding for wavy cylinders at sub-critical Reynolds numbers.

Lam et al. (2007) showed that the periodic wake distribution occurs on a row of side by side wavy cylinders along the spanwise direction. To validate the accuracy of the present computational domain height and the periodic boundary conditions on wavy tube bundles, a row of side by side wavy cylinders ($\lambda/D_m = 6$, $a/D_m = 0.15$) with a fixed spacing ratio of $1.5D_m$ was computed. Two wavy cylinder row cases with different computational domain heights were compared. As shown in Fig. 5a, the normalized time averaged streamwise velocity distributions of the wavy cylinder row in y–z plane at the positions of $x/D_m = 1.5$, 4, 6, and 8 show periodic velocity distribution repeatedly in z-direction with the computational domain height of 2λ. Moreover, the velocity distributions of the cylinder row with the computational domain height of 1λ show similar characteristics as that of the case with 2λ heights. It confirmed that the periodic boundary condition with only one spanwise wavelength in the computational domain is sufficiently accurate to simulate flow pass tube bundles with wavy cylinders arranged at the first row.

4.2. Velocity and turbulence intensity distributions

The accuracy of the computational results using LES is highly dependent on the mesh size and cell numbers. The grid independence test must be carried out prior to extensive numerical simulations. With reference to Table 2, for each cylinder, the cell numbers were set at 80 and 96 around the cylinder circumference, which correspond to the cell numbers in x–y plane of 36,432 and 44,592, respectively. Uniform layers of 28 and 32 were adopted

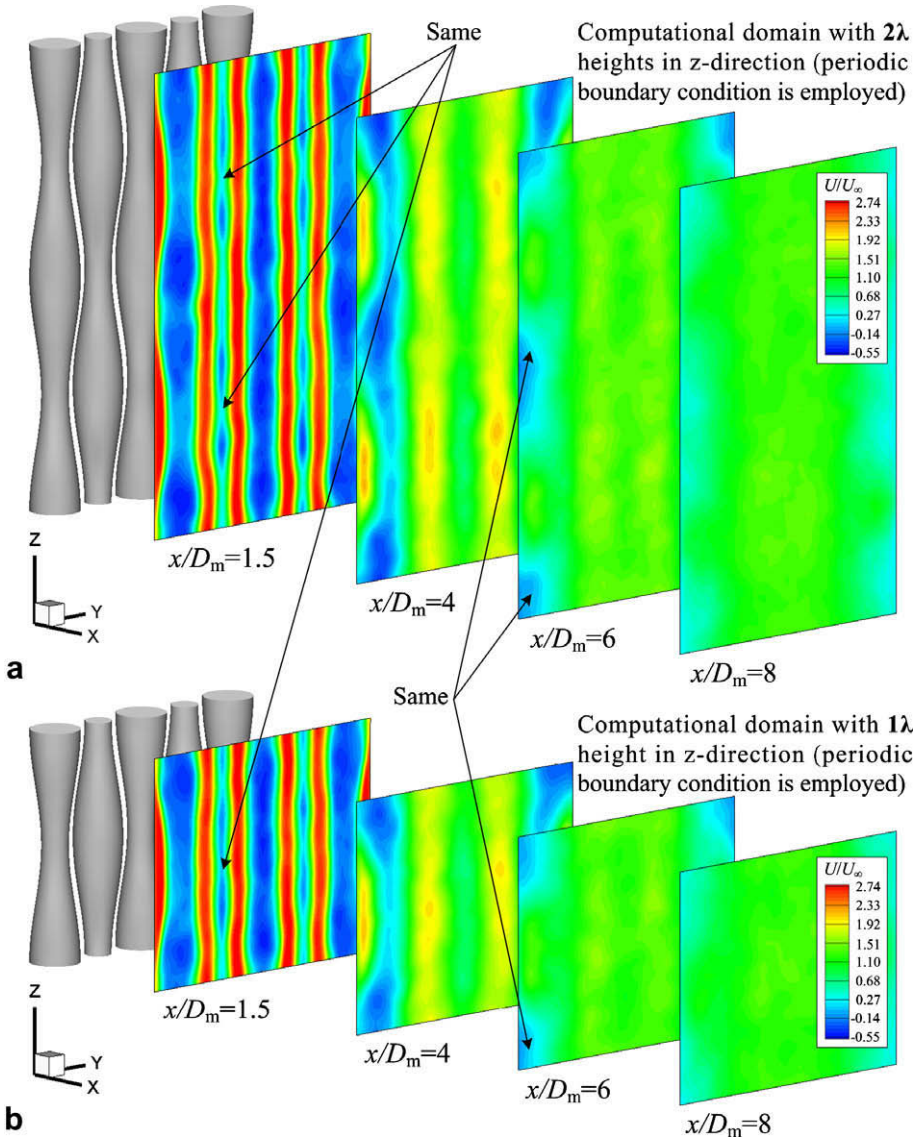

Fig. 5. Normalized time averaged streamwise velocity distributions in y–z plane at $x/D_m = 1.5$, 4, 6, and 8 for a row of wavy cylinders.

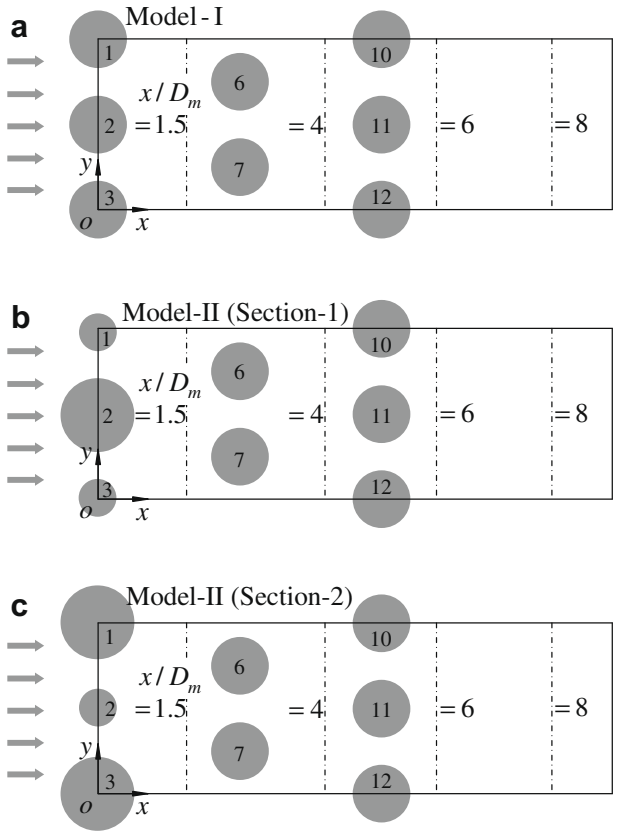

Fig. 6. Locations at which results are presented: $x/D_m = 1.5$, 4, 6, and 8.

for Model-I, Grid-I, and Grid-II, respectively. Uniform layers of 56 and 64 were used for Model-II, Grid-I, and Grid-II, respectively, because the computational domain along the spanwise direction for Model-II is double that of Model-I. Moreover, the validation tests of the present LES method were also performed by the comparison of the LES results with the LDA measurements on the tube bundles at the same Reynolds number of 7500. By using the LES method and LDA technique, the detailed velocity distributions at different positions (see Fig. 6) in the x–y planes were obtained.

Fig. 7 shows the mean streamwise velocity distributions at $x/D_m = 1.5$, 4, 6, and 8 for circular and wavy tube bundles (Model-I and Model-II), respectively. Both the present LES results by Grid-I and Grid-II show good agreement with the LDA measurements. The gap velocities behind the second row (position of $x/D_m = 4$) of tubes are evidently smaller than those behind the first row (position of $x/D_m = 1.5$) and the third row (position of $x/D_m = 6$) of tubes. However, no prominent difference in mean streamwise velocity distributions can be observed between those of tube bundles Model-I (first row with circular cylinders, CY) and Model-II (first row with wavy cylinders, WY: $\lambda/D_m = 6$, $a/D_m = 0.15$). This implies that the drag may not be significantly reduced by using either circular cylinders or wavy cylinders in the first row of tube bundles. At $x/D_m = 1.5$, the velocity distribution in Section 1 (see Fig. 7e) is slightly different from that in Section 2 (see Fig. 7i) for the tube bundles Model-II. Similar flow characteristics are also observed for the time averaged transverse velocity distributions as shown in Fig. 8. This may be due to the periodic wake structure along the spanwise direction of the wavy cylinder. At the further downstream positions ($x/D_m = 8$), no evident gap velocity is generated as the turbulent vortices amalgamate with each other. All these can be easily observed by the vortex structures to be discussed later.

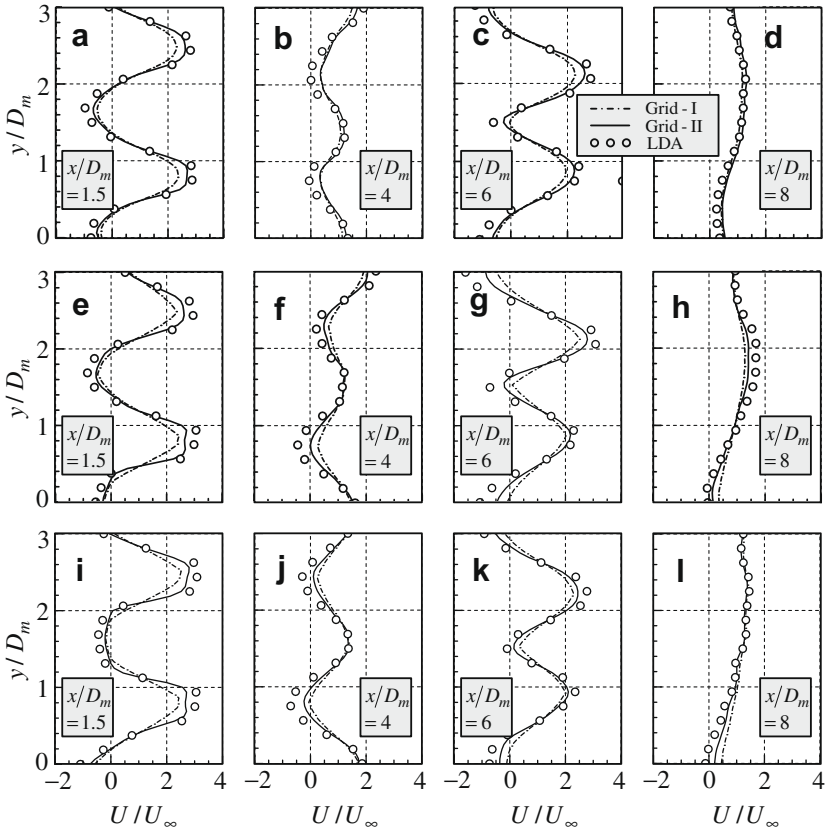

Fig. 7. Normalized time averaged streamwise velocity distributions for tube bundles Model-I and Model-II: (a–d) Model-I, first row with circular cylinders; (e–h) Model-II in Section 1, first row with wavy cylinders ($\lambda/D_m = 6$, $a/D_m = 0.15$); (i–l) Model-II in Section 2.

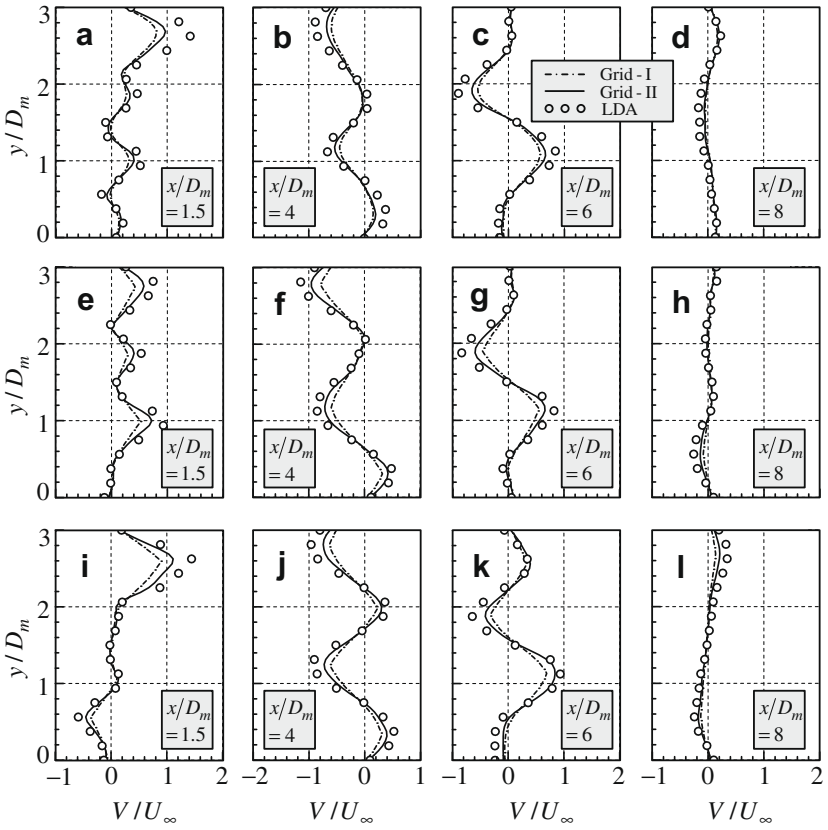

Fig. 8. Normalized time averaged transverse velocity distributions for tube bundles Model-I and Model-II: (a–d) Model-I, first row with circular cylinders; (e–h) Model-II in Section 1, first row with wavy cylinders ($\lambda/D_m = 6$, $a/D_m = 0.15$); (i–l) Model-II in Section 2.

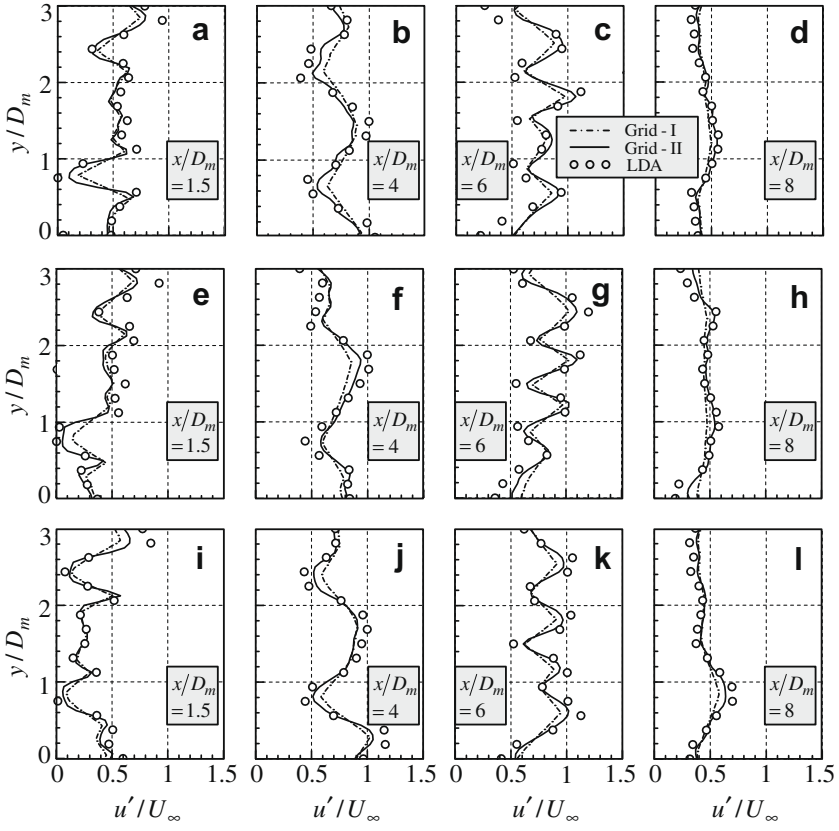

Fig. 9. Normalized time averaged streamwise turbulence intensity distributions for tube bundles Model-I and Model-II: (a–d) Model-I, first row with circular cylinders; (e–h) Model-II in Section 1, first row with wavy cylinders ($\lambda/D_m = 6$, $a/D_m = 0.15$); (i–l) Model-II in Section 2.

The time averaged turbulence intensity distributions of the tube bundles by LES method are also consistent with LDA results (see Figs. 9 and 10). The turbulence intensities u'/U_∞, v'/U_∞ are calculated by using the rms value of streamwise or transverse fluctuating velocity divided by U_∞ and neglecting SGS energy. At $x/D_m = 1.5$, the evident reduction of streamwise turbulence intensity occurs at Section 2 of the tube bundle Model-II compared with those of purely circular tubes (tube bundle Model-I) as shown in Fig. 9. This implies the weakness of vortex shedding behind the wavy tube arrays (WY: $\lambda/D_m = 6$, $a/D_m = 0.15$), which leads to the reduction of flow-induced vibration. Due to the three-dimensional periodic wake structure behind the wavy cylinder, the streamwise turbulence intensity shows a difference between Sections 1 and 2 for tube bundle Model-II. At x/D_m locations of 4, 6 and 8, this kind of difference becomes less distinct. As shown in Fig. 10, the time averaged transverse turbulence intensity at the location $x/D_m = 1.5$ of the tube bundle Model-II is also smaller than that of the tube bundle Model-I, especially for that in the Section 2. In general, the turbulence intensity behind the first row of wavy tubes (WY: $\lambda/D_m = 6$, $a/D_m = 0.15$) is smaller than that behind the second and third row of tubes (CY). The rms value of transverse velocity appears to be quite high as shown in Fig. 10. This may be due to the wall effect on such tube bundles. The severe interaction of vortices at such smaller spacing ratio for the present configuration (1.5, in crosswise direction, and 2.5 in streamwise direction) is another important reason for the high value of fluctuating transverse velocity. From the grid independence test and the validation of the present LES method, we concluded that with the present grid resolution, the LES method can predict the characteristics of turbulent flow past tube bundles accurately. To ensure better results and capture detailed vortex structures, the finer Grid-II is adopted for all the cases of the present tube bundles simulation.

4.3. Flow patterns and turbulent kinetic energy

The results above gave us reasonable confidence on the application of LES model to capture and study the complex turbulent flow characteristics past tube bundles. An extensive investigation on flow characteristics using LES method was carried out. The instantaneous and mean velocity field, vorticity field, and force characteristics can be extracted from the time dependent numerical simulation results for further analysis. Lam et al. (2007) investigated turbulent flow past a row of wavy cylinders. The results showed that the wavy cylinder arrays ($\lambda/D_m = 1.5$, $a/D_m = 0.15$) give rise to a more stable flow pattern with less fluctuation and longer wake vortex closure length compared with a row of circular cylinders. In the present simulations, refer to Table 1, a new tube bundle Model-III (wavy cylinders in the first row, WY: $\lambda/D_m = 1.5$, $a/D_m = 0.15$) is also introduced for further discussions using the LES method. The finer Grid-II and the computational domain for Model-I is also adopted for Model-III tube bundles.

As known to all, the vortex shedding phenomenon is associated with flow separation of the boundary layer from bluff bodies. For a wavy cylinder with smaller wavelength $\lambda/D_m = 1.5$, the flow separated quickly at the saddle positions than that at the nodal positions (Lam and Lin, 2008, 2009). The vortices in the saddle plane expand along both the streamwise and crosswise direction. It gives rise to a wide wake at the further downstream position. The vortices in the nodal plane seem to extend only in the streamwise direction and noticeably being suppressed in the crosswise direction. As a result, it produces a narrower wake. For wavy cylinder with large wavelength $\lambda/D_m = 6$, however, the flow separation occurs firstly at the nodal position and the flow patterns in nodal or saddle planes are opposite to those of the wavy cylinder with a smaller wavelength (Lam and Lin, 2009). Due to the effect of wavy tubes

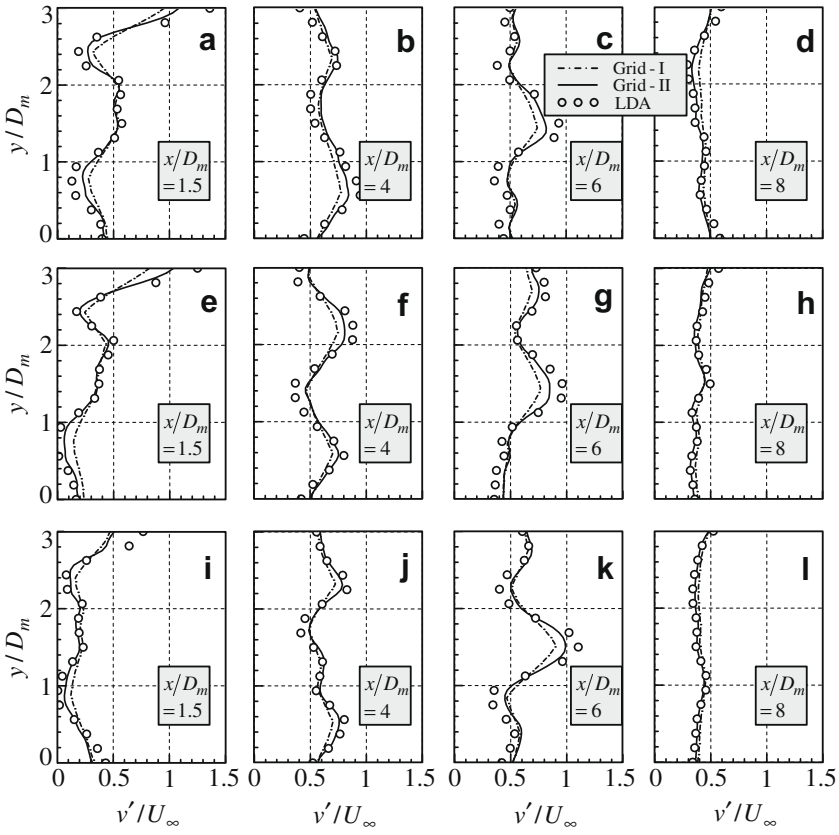

Fig. 10. Normalized time averaged transverse turbulence intensity distributions for tube bundles Model-I and Model-II: (a–d) Model-I, first row with circular cylinders; (e–h) Model-II in Section 1, first row with wavy cylinders ($\lambda/D_m = 6$, $a/D_m = 0.15$); (i–l) Model-II in Section 2.

arranged at the first row (Model-II, III), the wake patterns have been modified compared with those for tube bundle Model-I. As shown in Fig. 11, along the spanwise direction, the normalized time averaged streamwise velocity distributions in y–z plane at the position of $x/D_m = 1.5$ (between the first row and second row of tubes), $x/D_m = 4$ (between the second row and third row of tubes), $x/D_m = 6$ and 8 (behind the third row of tubes) are plotted. Compared with the tube bundle Model-I with purely circular

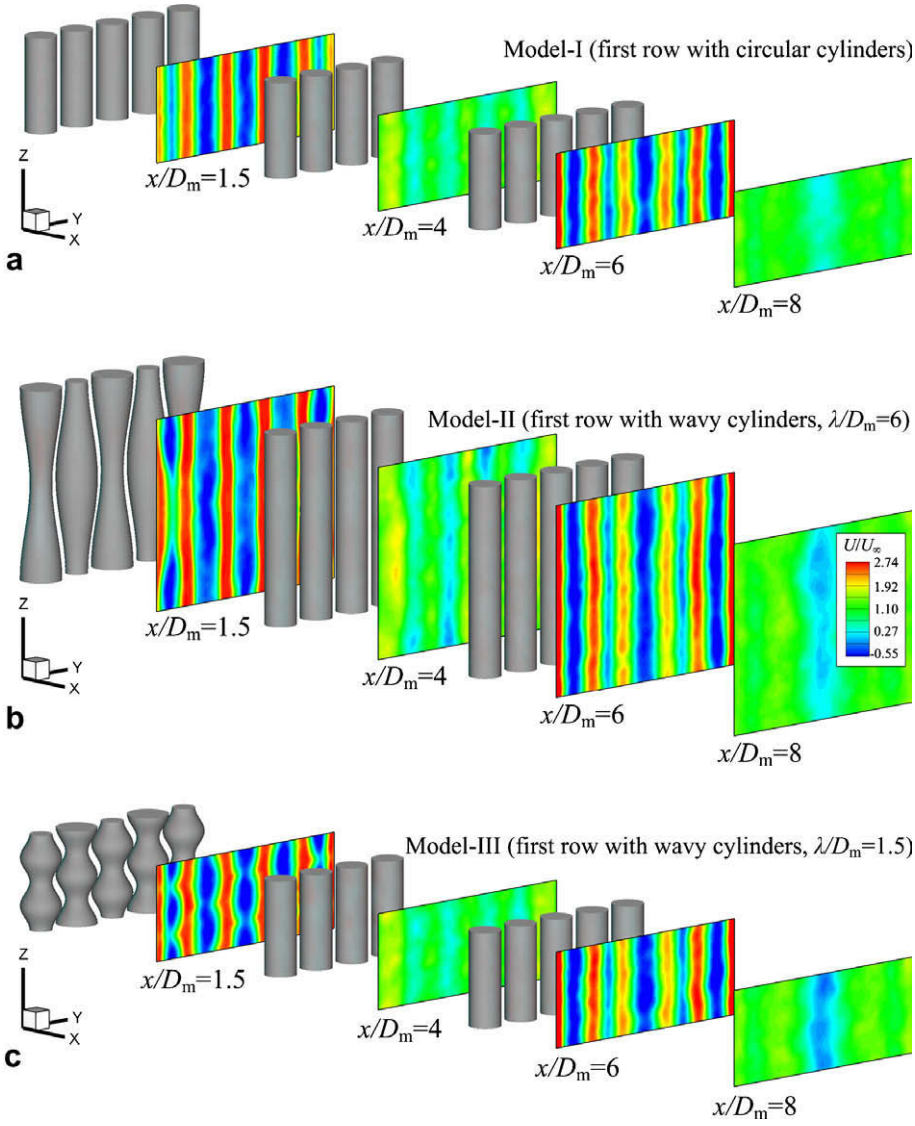

Fig. 11. Normalized time averaged streamwise velocity distributions in y–z plane at $x/D_m = 1.5$, 4, 6, and 8 for different tube bundles.

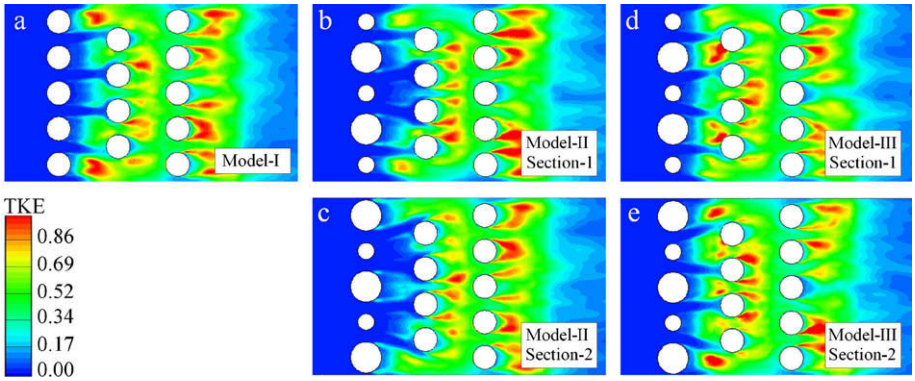

Fig. 12. Normalized turbulent kinetic energy (TKE) distributions for tube bundles at different locations.

cylinders, the streamwise velocity distributions shows periodic repeats along the spanwise direction for wavy tube bundles Model-II and III at $x/D_m = 1.5$. The negative value of streamwise velocity behind the nodal positions is larger than that behind the saddle positions for tube bundle Model-II with a large wavelength $\lambda/D_m = 6$, while the maximum negative streamwise velocity is observed behind the saddle positions for tube bundle Model-III with a smaller wavelength $\lambda/D_m = 1.5$. This is due to the different flow separation characteristic for different wavy cylinders. The spanwise periodic velocity distribution shows a more well organized wake structure behind the wavy tube arrays. At further downstream of $x/D_m = 4$, 6 and 8 behind the second and the third row of circular tubes, the periodic velocity variation disappeared along the spanwise direction and was replaced with the parallel lines distributions in the z-direciton.

Fig. 12 shows the contour plots of the normalized turbulent kinetic energy (TKE) in the x–y planes [TKE=$(u'^2 + v'^2 + w'^2)/2U_\infty^2$] of the wake behind the tube bundles Model-I, II, and III. Compared with the characteristics for circular tubes in the first row, the region of negligible turbulent kinetic energy is noticeably larger behind the wavy tubes Model-II (WY: $\lambda/D_m = 6$, $a/D_m = 0.15$). All the TKE values for different planes of the tube bundle Model-II are smaller than that with purely circular tube bundle. This suggests that this kind of wavy geometry can significantly reduce the TKE in the near wake. Likewise, with the turbulence intensity characteristics shown in Figs. 9 and 10, the reduction of TKE means that the fluctuating force exerted on the second tube row will be weakened and in turn, the vibration will be suppressed. It can be concluded that the fluctuating lift coefficients of the second row tubes for tube bundle Model-II are smaller than those for tube bundles Model-I (CY). However, no significant difference of the TKE between the tube bundle Model-I and Model-III (WY: $\lambda/D_m = 1.5$, $a/D_m = 0.15$) was observed.

4.4. Force characteristics and Strouhal numbers

Fig. 13a shows the drag coefficients $\bar{C}_D$ of the three different tube bundles predicted by the LES method. In general, the mean drag coefficients for wavy tubes (Model-II, first row with wavy cylinder: $\lambda/D_m = 6$, $a/D_m = 0.15$ and Model-III, first row with wavy cylinder: $\lambda/D_m = 1.5$, $a/D_m = 0.15$) show no significant reduction compared to the case of purely circular tubes. Similarly, there is no effect on the second and third rows. Lam et al. (2004b) reported that an elongation of the formation length for wavy cylinder will give rise to a higher back pressure in the rear side of a single cylinder, which is the main reason for producing a low drag force. It would be interesting to see whether the wavy cylinders will bring about the same effects on tube bundles. However, the present results show that this characteristic for drag force reduction is not generated by the wavy tube bundles at such small spacing ratio. Lam and Lin (2009) pointed out the typical spanwise waviness of wavy cylinder may lead to additional vorticity components which will give rise to two types of rib-like wake structures at the saddle or nodal positions. It modified the flow separation along the spanwise direction of the cylinder. As a result, the free shear layers extend to further downstream position and thus lead to the reduction of drag as a result of the longer vortex formation length. For wavy tube bundles, when the gap between side by side wavy cylinders is small, it will lead to a high value of velocity occurring in the gap. The high velocity jet flapping in the gap may distort and even suppress the well organized additional vorticity components that are generated in the case of a single wavy cylinder. It means that the phenomenon of longer vortex formation length disappears. This is the physical reason why there is no drag reduction for wavy tube bundles at such configuration compared with a single wavy cylinder. Due to the wall effect, the values of $\bar{C}_D$ for each tube in rows-1, 2, and 3 are generally different. For example, the value of $\bar{C}_D$ for cylinders 1 and 10 are much larger than that of the cylinders 3 and 12, respectively. In general, the values of $\bar{C}_D$ for each cylinder in tube row 1 and row 3 are significantly higher than that of a single circular or wavy cylinder at the same Reynolds number. The high value of $\bar{C}_D$ is mainly because of the blockage effect on the cylinders in heat exchangers due to the existence of side walls. Moreover, the configuration effects of staggered arrangement of the tube bundles with the streamwise and transverse pitch-to-diameter ratio of 2.5 and 1.5, respectively may also have effect on the increase of drag force on the cylinders. Schneider and Farge (2005) numerically simulated the staggered tube bundles at Re = 200 with the spacing ratio around 2.8 in both the streamwise direction and the crosswise direction. For the tube bundle with circular cylinders, the value of $\bar{C}_D$ is 3, which is two times more than that of a single circular cylinder at Re = 200. Furthermore, for the tube bundle with square cylinders, the value of $\bar{C}_D$ is 18.8 which is much higher than that of a single square cylinder. Kumar et al. (2008) showed that a row of square cylinder with spacing ratio of two (crosswise direction), the

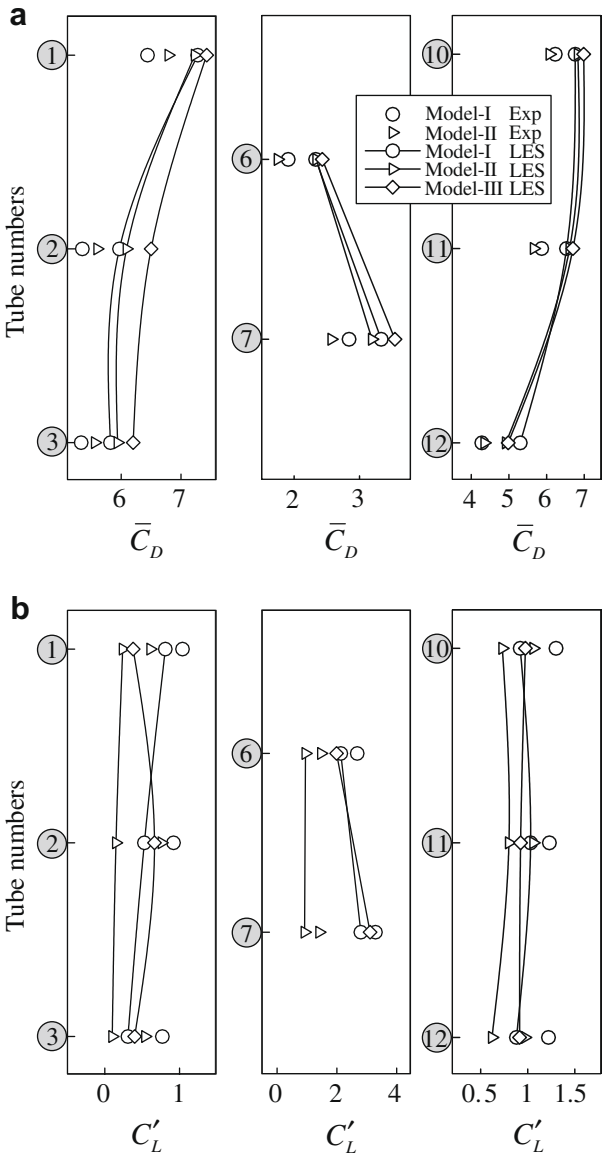

Fig. 13. Mean drag coefficients and fluctuating lift coefficients for tube bundles obtained by LES method and the load cell measurements at sub-critical Reynolds numbers of Re = 7500.

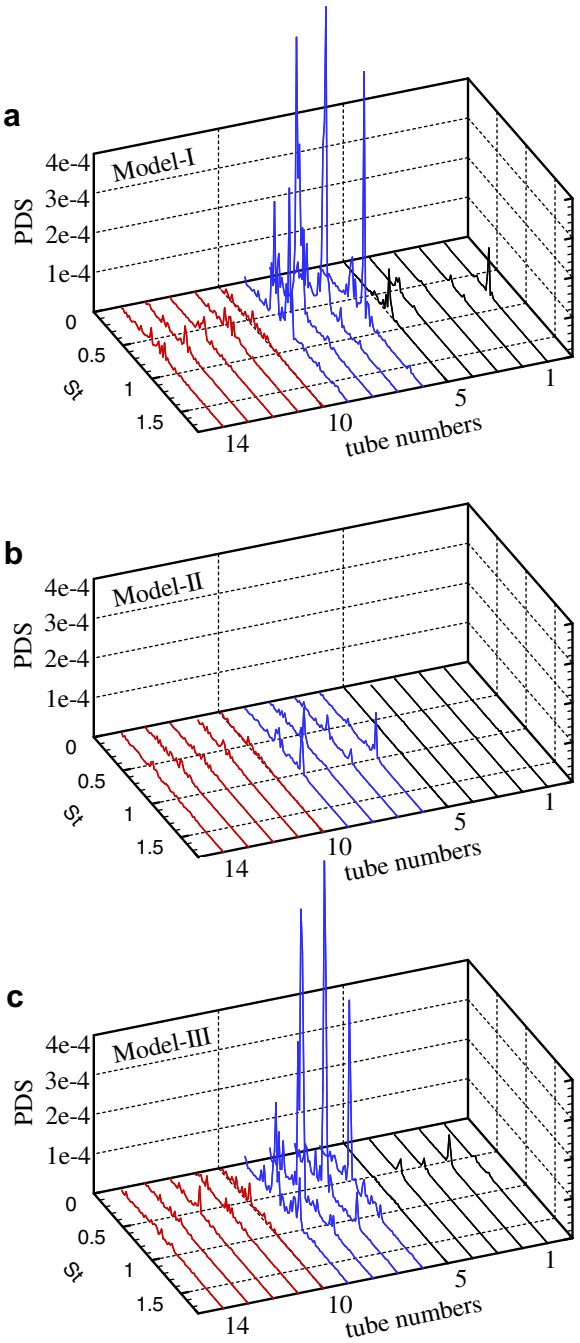

Fig. 14. Normalized lift force power spectrum for tube bundles at Re = 7500 by LES results.

value of $\bar{C}_D$ up to 6.5 was obtained at a low Reynolds number of 80. Increasing the spacing ratio to 5, the value of $\bar{C}_D$ is reduced to 2. All the results show that the drag force on tube bundle has stronger relationship with the configuration of the cylinders. A smaller spacing ratio may lead to a higher value of drag coefficient. In general, the closer the cylinders were packed, the higher the drag coefficient that would be obtained. The exact value will depend on the actual configuration.

Moreover, some interesting results are obtained concerning the fluctuating lift coefficients C_L' (see Fig. 13b). The present results show that the out-of-phase arranged wavy tubes (WY: $\lambda/D_m = 6$, $a/D_m = 0.15$) give rise to a more stable flow pattern with less fluctuation; especially in the second row of tubes (refer to Fig. 12). The fluctuating lift coefficients for the tube bundle Model-II are all less than those with purely circular tube bundle (Model-I), especially the effect on the second row of tubes. This demonstrates that the introduction of suitable wavy cylinders in the first row is an effective way for the control of FIV. The mean drag coefficient $\bar{C}_D$ and the fluctuating lift coefficient C_L' of each tube for both tube bundles Model-I (CY) and Model-II (WY: $\lambda/D_m = 6$, $a/D_m = 0.15$) using the load cell techniques are also plotted in Fig. 13 for comparison. The values of $\bar{C}_D$ by LES methods are slightly larger than those obtained from the load cell measurements, while C_L' shows large discrepancies between the LES and experimental results. The large discrepancy of C_L' may be due to the effect on the periodic boundary condition used by the present LES method (infinite cylinder length with repeating wavelength for the wavy cylinder) compared with the experimental results (finite length cylinders with an aspect ratios of 14.85). The two end plate set in the water tunnel may lead to the end wall effect on the tube bundles. As a result, it leads to a significant difference of force obtained by the load cell technique and the LES method, especially for the fluctuating lift (also, refer to Fig. 3 for single cylinder). However, the general characteristics obtained by LES method are consistent with the load cell measurements. That is to say, the present LES method can predict the force characteristics quite well although the exact value may depend on the experimental set up. Therefore, the values of $\bar{C}_D$ and C_L' of all the tubes were calculated for the investigation on the control of FIV.

In the present numerical simulation on tube bundles, the vortex shedding frequency was obtained by Fast Fourier Transform (FFT) of the time history of the lift coefficient. The values of Strouhal number ($St = f_s D_m/U_\infty$) for each circular or wavy tube are plotted in Fig. 14. Similar to the results of turbulent kinetic energy shown in Fig. 12 and the fluctuating lift coefficients in Fig. 13b, the power density spectra of vortex shedding in the tube bundle are evidently suppressed for the optimal wavy tubes introduced in the first row (tube bundle Model-II), when compared with the tube bundles Model-I and Model-III. Moreover, the Strouhal numbers of these three-dimensional tubes are all in the range of 0.5–1, which is close to the value of 0.72–1.3 found by Price et al. (1995) and 0.92–1.18 by Kevlahan and Wadsley (2005). This also confirms that a heat exchanger tube bundle composed of circular and some typical wavy cylinder with optimal wavelength may have advantages in the control of flow-induced vibration of the tube bundles.

5. Conclusions

The effects of introducing a row of wavy cylinders with suitable wavelength into circular tube bundles for the control of flow-induced vibration were investigated. To identify the suitable wavy cylinder, both the experimental and numerical investigations on flow around a wavy cylinder with a wavelength of $\lambda/D_m = 6$ and $a/D_m = 0.15$ was carried out, first at the sub-critical Reynolds numbers range from 6800 to 13,400. Significant drag reduction and the fluctuating lift suppression of the wavy cylinder were found in such Reynolds numbers range, similar to that occurring in the laminar flow conditions. Upon confirmation of optimal wavelengths, both experimental measurements and large eddy simulation (LES) technique were used to study the turbulent flow characteristics around the staggered tube bundles arrangement composed of different combinations of wavy cylinders and circular cylinder at sub-critical Reynolds number Re = 7500. LDA technique was used to capture the velocity distributions. The numerical results agree quite well with the experimental measurements. It confirms that with carefully designed grid resolution and distribution, the LES method can predict accurately the characteristics of turbulent flow past heat exchanger tube bundles. Therefore, the instantaneous

and mean velocity field, vorticity field and force characteristics which are very difficult to obtain experimentally in heat exchanger tube bundles, are extracted from the numerical simulation results for the analysis of the complex flow characteristics in tube bundles.

In the present study, two types of tube bundles with the first row of circular tubes replaced by different wavy cylinders (Models-II and III) are studied and the results are compared with that of purely circular cylinders at the Reynolds number of 7500. When the first row of tubes is replaced by wavy cylinders, in general, the drag is not evidently reduced by using such combination. However, the fluctuating lift is significantly weakened for the wavy tube bundle of Model-II (WY) with wavy cylinders $\lambda/D_m = 6$ and $a/D_m = 0.15$ placed in the first row. Because of the introduction of this kind of wavy tubes at the first row (Model-II), the turbulent kinetic energy behind the first row tubes are reduced and the wake patterns of the second row tubes are more well organized compared with the tube bundle with purely circular cylinders (Model-I) and the tube bundle with wavy cylinders (Model-III, WY: $\lambda/D_m = 1.5$, $a/D_m = 0.15$) placed in the first row. The power density spectra of the vortex shedding in the tube bundle are evidently suppressed. This implies that the turbulent forces on the second tube row are weakened. It is concluded that by introducing a suitable wavy cylinders in tube bundles (such as tube bundle Model-II), some good effects on the control of flow-induced vibration of the tube bundles in the heat exchanger can be achieved.

Acknowledgement

The authors wish to thank the Research Grants Council of the Hong Kong Special Administrative Region, China, for its support through Grant No. PolyU 5188/05E.

References

Austermann, R., Popp, K., 1995. Stability behaviour of a single flexible cylinder in rigid tube arrays of different geometry subjected to cross-flow. J. Fluid. Struct. 9, 303–322.

Balabani, S., Yianneskis, M., 1996. An experimental study of the mean flow and turbulence structure of cross-flow over tube bundles. Proc. IMechE Part C, J. Mech. Eng. Sci. 210, 317–331.

Barsamian, H.R., Hassan, Y.A., 1997. Large eddy simulation of turbulent cross flow in tube bundles. Nucl. Sci. Eng. 172, 103–122.

Beale, S.B., Spalding, D.B., 1999. A numerical study of unsteady fluid flow in in-line and staggered tube banks. J. Fluid. Struct. 13, 723–754.

Bearman, P.W., Owen, J.C., 1998. Reduction of bluff-body drag and suppression of vortex shedding by the introduction of wavy separation lines. J. Fluid. Struct. 12, 123–130.

Bouris, D., Bergeles, G., 1999. Two dimensional time dependent simulation of the subcritical flow in a staggered tube bundle using a subgrid scale model. Int. J. Heat Fluid Flow 20, 105–114.

Breuer, M., 1998. Large eddy simulation of the subcritical flow past a circular cylinder: numerical and modeling aspects. Int. J. Numer. Meth. Fluids 28, 1281–1302.

Chen, S.S., Srikantiah, G.S., 2001. Motion-dependent fluid force coefficients for tube arrays in crossflow. ASME J. Press. Vess. Technol. 123, 429–436.

Darekar, R.M., Sherwin, S.J., 2001. Flow past a square-section cylinder with a wavy stagnation face. J. Fluid Mech. 426, 263–295.

Kevlahan, N.K.-R., Wadsley, J., 2005. Suppression of three-dimensional flow instabilities in tube bundles. J. Fluid Struct. 20, 611–620.

Kumar, S.R., Sharma, A., Agrawal, A., 2008. Simulation of flow around a row of square cylinders. J. Fluid Mech. 606, 369–397.

Lam, K., Lin, Y.F., 2007. Drag force control of flow over wavy cylinders at low Reynolds number. J. Mech. Sci. Technol. 21, 1331–1337.

Lam, K., Lin, Y.F., 2008. Large eddy simulation of flow around wavy cylinders at a subcritical Reynolds number. Int. J. Heat Fluid Flow 29, 1071–1088.

Lam, K., Lin, Y.F., 2009. Effects of wavelength and amplitude of a wavy cylinder in cross-flow at low Reynolds numbers. J. Fluid Mech. 620, 195–220.

Lam, K., Wang, F.H., Li, J.Y., So, R.M.C., 2004a. Experimental investigation of the mean and fluctuating forces of wavy (varicose) cylinders in a cross-flow. J. Fluid. Struct. 19, 321–334.

Lam, K., Wang, F.H., So, R.M.C., 2004b. Three-dimensional nature of vortices in the near wake of a wavy cylinder. J. Fluid Struct. 19, 815–833.

Lam, K., Jiang, G.D., Liu, Y., So, R.M.C., 2006. Simulation of cross-flow induced vibration of cylinder arrays by surface vorticity method. J. Fluid Struct. 22, 1113–1131.

Lam, K., Cai, T., Lin, Y.F., Liu, Y., 2007. Flow characteristics around a row of circular and wavy cylinders. J. Mech. Sci. Technol. 21, 1910–1917.

Liang, C., Papadakis, G., 2007. Large eddy simulation of cross-flow through a staggered tube bundle at subcritical Reynolds number. J. Fluid Struct. 23, 1215–1230.

Norberg, C., 2003. Fluctuating lift on a circular cylinder: review and new measurements. J. Fluid Struct. 17, 57–96.

Paul, S.S., Tachie, M.F., Ormiston, S.J., 2007. Experimental study of turbulent cross-flow in a staggered tube bundle using particle image velocimetry. Int. J. Heat Fluid Flow 28, 441–453.

Paul, S.S., Ormiston, S.J., Tachie, M.F., 2008. Experimental and numerical investigation of turbulent cross-flow in a staggered tube buddle. Int. J. Heat Fluid Flow 29, 387–414.

Price, S.J., Paidoussis, M.P., Mark, B., 1995. Flow visualization of the interstitial cross-flow through parallel triangular and rotated square arrays of cylinders. J. Sound Vib. 181, 85–98.

Rollet-Miet, P., Laurence, D., Ferziger, J., 1999. LES and RANS of turbulent flow in tube bundles. Int. J. Heat Fluid Flow 20, 241–254.

Romberg, O., Popp, K., 1998a. The influence of trip-wires on the fluid damping-controlled instability of a flexible tube in a bundle. J. Fluid Struct. 12, 17–32.

Romberg, O., Popp, K., 1998b. The influence of upstream turbulence on the stability boundaries of a flexible tube in a bundle. J. Fluid Struct. 12, 153–169.

Rottmann, M., Popp, K., 2003. Influence of upstream turbulence on the fluidelastic instability of a parallel triangular tube bundle. J. Fluid Struct. 18, 595–612.

Schneider, K., Farge, M., 2005. Numerical simulation of the transient flow behaviour in tube bundles using a volume penalization method. J. Fluid Struct. 20, 555–566.

Sohankar, A., Davidson, L., Norberg, C., 2000. Large eddy simulation of flow past a square cylinder: comparison of different subgrid scale models. J. Fluid Struct. 122, 39–47.

Sweeney, C., Meskell, C., 2003. Fast numerical simulation of vortex shedding in tube arrays using a discrete vortex method. J. Fluid Struct. 18, 501–512.

Wang, Z.J., Zhou, Y., Huang, J.F., Xu, Y.L., 2005. Fluid dynamics around an inclined cylinder with running water rivulets. J. Fluid Struct. 21, 49–64.

Watterson, J.K., Dawes, W.N., Savill, A.M., White, A.J., 1999. Predicting turbulent flow in a staggered tube bundle. Int. J. Heat Fluid Flow 20, 581–591.

Williamson, C.H.K., 1996. Vortex dynamics in the cylinder wake. Annu. Rev. Fluid Mech. 28, 477–539.

Williamson, C.H.K., Wu, J., Sheridan, J., 1995. Scaling of streamwise vortices in wakes. Phys. Fluids 7, 2307–2309.

Zdravkovich, M.M., 1997. Flow Around Circular Cylinders. Fundamentals, vol. 1. Oxford University Press.

Zhang, W., Dai, C., Lee, S.J., 2005. PIV measurements of the near-wake behind a sinusoidal cylinder. Exp. Fluids 38, 824–832.